

Secrecy performance of FSO communication systems with non-zero boresight pointing errors

Gyan Deep Verma¹ | Aashish Mathur¹ | Yun Ai²  | Michael Cheffena²

¹ Department of Electrical Engineering, Indian Institute of Technology Jodhpur, Jodhpur, India

² Faculty of Engineering, Norwegian University of Science and Technology, Gjøvik, Norway

Correspondence

Aashish Mathur, Department of Electrical Engineering, Indian Institute of Technology Jodhpur, Jodhpur, 342037, India.
Email: aashishmathur@iitj.ac.in

Abstract

Free space optical (FSO) communication is a promising candidate for the next generation (5G and beyond) wireless communication systems, due to its merits (i.e. low latency, high data rate, and license-free band, among others). However, atmospheric turbulence (AT) as well as pointing error (PE) are two of the main challenges with FSO communication that affect its performance. Here, the exact closed-form expression of the average secrecy capacity and secrecy outage probability under the composite effect of AT and non-zero boresight PEs is evaluated. For all the regimes of the AT (weak to strong), a generalised Malaga distribution is used to model the channel fading gain of the FSO link. The expressions are generalised and valid for all turbulence, and are applicable for intensity modulation direct detection as well as heterodyne detection techniques.

1 | INTRODUCTION

Free space optical (FSO) communication has many advantages such as the license-free band, high data rate, low latency, and quick deployability, among others [1]. Despite its aforementioned merits the performance of FSO system is limited by atmospheric turbulence (AT) and pointing error (PE). As the solar radiation reaches the surface of the Earth, the air near the Earth's surface has higher temperature compared to the air at relatively higher altitudes. The warmer air rises to mix turbulently with the surrounding cooler air which results in the random temperature fluctuations. This temperature variation leads to inhomogeneities in the medium thereby resulting in the formation of discrete cells or eddies of different sizes and refractive indices. The interaction of the transmitted laser beam with this turbulent path generates random fluctuations in the amplitude and phase of the received signal. This phenomenon is called AT which results in corresponding intensity fluctuations and leads to system performance degradation, especially in long distance transmission of about several kilometers [1–3].

In addition, there might be a degradation in the performance due to slight misalignment between the transmitter (Tx) and the receiver (Rx), caused by for example, swaying buildings, vibrations, and thermal expansion of the building, which leads to beam pointing errors (PEs). PEs represent the horizontal and

vertical displacement along the laser beam; both these components are assumed to follow independent Gaussian distribution [4]. PE has two components: jitter and boresight. Jitter is the random offset of the beam and the detector plane mainly caused by dynamic wind load, weak earthquake, and swaying buildings. Boresight refers to the fixed displacement between the beam center and the detector center caused by thermal expansion [5]. It was established in [6] that PE is a serious issue in urban areas and the effect of PE was experimentally demonstrated.

Conventionally, FSO systems utilise intensity modulation direct detection (IM/DD) due to the low cost and ease of implementation, contrary to heterodyne detection (HD) technique which has a higher cost and is relatively difficult to implement. In HD technique, a robust oscillator field mixes with the received signal which provides much better spatial and frequency selectivity than IM/DD. Furthermore, HD technique can recover the information from amplitude, phase, or polarisation from the received signal, which improves the spectral efficiency and FSO system performance. Another main advantage of HD technique is that it can overcome thermal noise [7, 8]. Nevertheless, both detection techniques are used as per application and cost.

Inherently FSO communication is more secure than radio frequency (RF) communication because the optical beams are more directional compared to the RF beams thus less subject to

This is an open access article under the terms of the [Creative Commons Attribution](https://creativecommons.org/licenses/by/4.0/) License, which permits use, distribution and reproduction in any medium, provided the original work is properly cited.

© 2020 The Authors. *IET Communications* published by John Wiley & Sons Ltd on behalf of The Institution of Engineering and Technology

eavesdropping/intercepting. However, optical beams can be still intercepted. In [9], two possible cases to intercept the laser beam have been mentioned. In the first scenario, when the eavesdropper is located close to the Tx, the potential eavesdropper cannot intercept the beam without partially blocking the line-of-sight (LOS) between the legitimate Tx and Rx due to the narrowness of the laser beam near the Tx. In order to intercept the beam, a sufficiently sophisticated device such as a beam splitter is required by the eavesdropper to collect fractional power of the transmitted beam. In the second scenario, the eavesdropper is located near the legitimate Rx. The laser beam usually experiences divergence due to optical diffractions. Thus, the eavesdropping is possible in FSO systems when the location of eavesdropper lies in the divergence region of the laser beam. This is one of the most probable ways of eavesdropping in FSO communication systems. In recent few years, research on the physical layer security (PLS) has been increased significantly [10].

Data encryption is one way to secure the data, but it leads to higher bandwidth consumption as well as increased complexity in upper layer [9]. PLS is a complimenting solution to securing the communication in the presence of eavesdroppers [9, 11]. In this regard, PLS is widely considered as a promising technique to enhance secrecy in next generation (5G and beyond) communication systems [12, 13]. In [14], analysis on average secrecy capacity (ASC) and secrecy outage probability (SOP) analysis have been done for hybrid satellite-FSO cooperative systems. In [15], ASC and SOP performance metrics have been analysed under Malaga AT but the effect of boresight PEs have been ignored. In [16], analytical expressions of ASC and SOP are derived for a single-input multiple-output (SIMO) simultaneous wireless information and power transfer (SWIPT) based mixed RF/FSO communication system, where the RF link is characterised by Nakagami- m fading and the FSO link follows Malaga distribution. Similarly, in [17], the author's evaluated the PLS performance for a two-way relay based mixed RF/FSO network assuming similar channel models as in [16], but ignored the effects of non-zero boresight. Thereafter, the PLS performance for a mixed RF/FSO system under Gamma-Gamma AT model with PE (only jitter) has been analysed in [18]. It is clear from the above papers and the references therein that the effect of boresight PEs have not been considered when evaluating the PLS of FSO communication systems despite its non-ignorable impact on the system performance. In this regard, the main contributions of this paper are as follows:

- 1) We derive an exact closed-form expression of ASC under the composite effect of AT and PEs (jitter and boresight) contrary to [15], where only the jitter effect is considered.
- 2) An exact closed-form expression of SOP under the combined influence of AT and PEs (jitter and boresight) has been evaluated contrary to [15], where only lower bound of SOP is obtained.
- 3) The derived ASC and SOP expressions are generalised and applicable to both IM/DD and HD techniques.
- 4) Some useful insights into the FSO secrecy performance are obtained through the asymptotic SOP analysis.

2 | SYSTEM DESCRIPTION

We assume a classical Wyner's wiretap model [19], in which Alice (A) is the Tx, Bob (B) is a legitimate Rx, and Eve (E) is an external eavesdropper. The legitimate (A-B) and eavesdropper (A-E) links experience Malaga distributed flat fading effects [3, 7]. PEs are introduced at the Rx due to misalignment between A and B. The received optical signal, after conversion into electrical signal using HD (coherent) or IM/DD (non-coherent) technique at the Rx, is given by

$$y = \eta_0 s I_g + w, \quad (1)$$

where η_0 is responsivity of the photodetector (hereinafter assumed unity), s represents the transmitted optical signal, $I_g = I_a I_p I_l$ is the FSO communication channel gain that consists of three components: (i) I_a denotes Malaga AT, which occurs due to inhomogeneities present along the transmission path that randomly changes the laser beam phase and amplitude at the Rx, (ii) I_p represents the PE attenuation considering the combined effects of jitter as well as non-zero boresight caused due to dynamic wind load, building sways, and thermal expansion in the high rise buildings, thereby resulting into misalignment between the Tx and Rx [2, 4], (iii) I_l indicates path loss which is a deterministic constant described by the Beer-Lambert's law and is a function of distance, visibility, and operating wavelength [4]. Since the investigation of the path loss parameter is not the prime focus of this research and as such it is a deterministic factor. Thus, without loss of generality, I_l is assumed to be unity [2, 20]. In (1), w represents additive white Gaussian noise (AWGN) with zero mean and power spectral density N_0 [14], which, without loss of generality, is assumed to be the same for both the links (legitimate and eavesdropper). The closed-form expression of the probability density function (PDF) of Malaga AT is expressed as [7, 21].

$$f_{I_a}(I_a) = A \sum_{k=1}^{\beta} a_k I_a^{\frac{\alpha+k-2}{2}} K_{\alpha-k} \left(2 \sqrt{\frac{\alpha \beta I_a}{g \beta + \Omega'}} \right), \quad I_a > 0, \quad (2)$$

$$A \stackrel{\Delta}{=} \frac{2 \alpha^{\frac{\alpha}{2}}}{g^{1+\frac{\alpha}{2}} \Gamma(\alpha)} \left(\frac{g \beta}{g \beta + \Omega'} \right)^{(\beta + \alpha/2)}, \quad (2.a)$$

$$\Omega' \stackrel{\Delta}{=} \Omega + 2b_0 \rho + 2\sqrt{2b_0 \rho} \cos(\phi_a - \phi_b), \quad (2.b)$$

$$a_k \stackrel{\Delta}{=} \binom{\beta-1}{k-1} \frac{(g \beta + \Omega')^{1-\frac{k}{2}}}{(k-1)!} \left(\frac{\Omega'}{g} \right)^{k-1} \left(\frac{\alpha}{\beta} \right)^{\frac{k}{2}}, \quad (2.c)$$

where $\alpha > 0$ is related to the effective number of large scale cells of the scattering process, β is a natural number¹ that

¹ We consider Malaga AT model with the assumption that β is a natural number. While [21] has considered β to be a real number which results into infinite summations in the derived expressions, the assumption of β being a natural number results into finite tractable summations with high accuracy in the expressions derived in this research work. The assumption of β to be a natural number is also considered in [7]. The analysis presented in this work can be extended on similar lines to include the case of β being a real number [2, 21].

represents the amount of fading, $2b_0$ represents the average power of total scatter components, $g = 2b_0(1 - \rho)$ indicates the average power of the scattering component received by off-axis eddies, $0 \leq \rho \leq 1$ is the amount of power coupled to the LOS component, Ω' denotes the average power from the coherent component, Ω is the average power of the LOS component, ϕ_a and ϕ_b are the deterministic phases of LOS and coupled to LOS scatter term, respectively, $K_\nu(\cdot)$ denotes the modified Bessel function of second kind and order ν , and $\Gamma(\cdot)$ represents Gamma function [22].

2.1 | PE model with non-zero boresight

The approximation of the Beckmann's distribution into modified Rayleigh distribution is described as [2, 4]

$$f_U(U) = \frac{U}{\sigma_{mod}^2} \exp\left(-\frac{U^2}{2\sigma_{mod}^2}\right), \quad U \geq 0, \quad (3)$$

where $U = [U_x, U_y]$ is the radial displacement vector, where U_x and U_y represent the horizontal and vertical displacement from the Rx plane and are modeled as independent Gaussian random variable (RV). Further, $U_x \sim N(\mu_x, \sigma_x^2)$, $U_y \sim N(\mu_y, \sigma_y^2)$, where μ_x and μ_y denotes horizontal and vertical boresights (mean) and σ_x^2 and σ_y^2 represent horizontal and vertical jitters (variance). The beam width $\omega_x \approx \theta z$, where θ is divergence angle and z is distance between Tx and Rx, $\nu = \frac{\sqrt{\pi}a}{\sqrt{2}w_x}$, $A_0 = [erf(\nu)]^2$ is the fraction of the collection power at $u = 0$, a is detector aperture radius and $\omega_{req}^2 = \frac{\omega_x^2 \sqrt{\pi} erf(\nu)}{2\nu \exp(\nu^2)}$ denotes the equivalent beam radius at the Rx. Some other PE's parameters are $\psi_x = w_{req}/(2\sigma_x)$, $\psi_y = w_{req}/(2\sigma_y)$, where ψ_x and ψ_y represent the ratio of the equivalent beam radius at the Rx and standard deviation with respective PE displacement at the Rx, $G = \exp\left(\frac{1}{\psi_{mod}^2} - \frac{1}{2\psi_x^2} - \frac{1}{2\psi_y^2} - \frac{\mu_x^2}{2\sigma_x^2\psi_x^2} - \frac{\mu_y^2}{2\sigma_y^2\psi_y^2}\right)$, $A_{mod} = A_0G$, and $\sigma_{mod}^2 = \left(\frac{3\mu_x^2\sigma_x^4 + 3\mu_y^2\sigma_y^4 + \sigma_x^6 + \sigma_y^6}{2}\right)^{\frac{1}{3}}$, $\psi_{mod} = \omega_{req}/(2\sigma_{mod})$. The PDF of PE with non-zero boresight is given by [4]

$$f_{I_p}(I_p) = \frac{\psi_{mod}^2}{(A_{mod})\psi_{mod}^2} I_p^{\psi_{mod}^2 - 1}, \quad 0 \leq I_p \leq A_{mod}. \quad (4)$$

2.2 | Composite effect of the AT and PE

Using (2) and (4), after applying RV transformation, the PDF of the instantaneous signal-to-noise ratio (SNR) under the combined effect of AT and non-zero boresight PE is given by [7]

$$f_{\gamma_x}(\gamma_x) = \frac{\psi_{mod_x}^2 A_x}{2^j \gamma_x} \sum_{k=1}^{\beta_x} b_{kx} \times G_{1,3}^{3,0} \left(\psi_{mod_x}^2 + 1 \left| \alpha_x, k \right. \left| B_x \left(\frac{\gamma_x}{\mu_{jx}} \right)^{\frac{1}{j}} \right), \quad (5)$$

where $x \in \{B, E\}$, $j = 1$ and $j = 2$ for HD and IM/DD, respectively, $b_{kx} = a_{kx} j^{(\alpha_x + k - 1)}$, $B_x = \frac{\psi_{mod_x}^2 \alpha_x \beta_x (g_x + \Omega'_x)}{(\psi_{mod_x}^2 + 1)(g_x \beta_x + \Omega'_x)}$ and μ_{jx} is electrical SNR established as $\mu_{jx} = \frac{(\eta_0 E[I_g])^j}{N_0}$, $E[I_g] = \frac{I_l A_{mod_x} \psi_{mod_x}^2 (g_x + \Omega'_x)}{(\psi_{mod_x}^2 + 1)}$, $E[\cdot]$ denotes the expectation operator, and $G_{p,q}^{m,n}(\alpha | a_1, \dots, a_p; b_1, \dots, b_q)$ represents the Meijier-G function. The PDF in (5) can be re-written in the following alternative form:

$$f_{\gamma_x}(\gamma_x) = \frac{D_x E_x}{\mu_{jx}} \sum_{k=1}^{\beta_x} b_{kx} G_{j,3j}^{3j,0} \left(l_{1x} - 1 \left| \frac{E_x \gamma_x}{\mu_{jx}} \right. \right), \quad (6)$$

where $D_x = \frac{\psi_{mod_x}^2 A_x}{2^j (2\pi)^{j-1}}$, $E_x = B_x^j / j^{2j}$, $l_{1x} = \frac{\psi_{mod_x}^2 + 1}{j}$, \dots , $\frac{\psi_{mod_x}^2 + j}{j}$ consists of j terms, $l_{2x} = \frac{\psi_{mod_x}^2}{j}, \dots, \frac{\psi_{mod_x}^2 + j - 1}{j}$, $\frac{\alpha_x}{j}, \dots, \frac{\alpha_x + j - 1}{j}, \frac{k}{j}, \dots, \frac{k + j - 1}{j}$ consists of $3j$ terms. Using (6), the cumulative distribution function (CDF) of the instantaneous SNR is found as

$$F_{\gamma_x}(\gamma_x) = D_x \sum_{k=1}^{\beta_x} b_{kx} G_{j+1,3j+1}^{3j,1} \left(\left(1, l_{1x} \left| \frac{E_x \gamma_x}{\mu_{jx}} \right. \right) \right). \quad (7)$$

3 | ASC PERFORMANCE ANALYSIS

ASC represents the maximum achievable secrecy rate of the legitimate link in the presence of active eavesdropper. The instantaneous secrecy capacity of the considered system can be defined as $C_s(\gamma_B, \gamma_E) = \max\{\log_2(1 + c_j \gamma_B) - \log_2(1 + c_j \gamma_E), 0\}$, where $c_1 = 1$ and $c_2 = e/(2\pi)$ for HD and IM/DD, respectively [15]. The ASC is, therefore, expressed as [23]

$$ASC = \int_0^\infty \int_0^\infty C_s(\gamma_B, \gamma_E) f(\gamma_B, \gamma_E) d\gamma_B d\gamma_E \quad (8)$$

$$= \frac{1}{\ln(2)} [I_1 + I_2 - I_3], \quad (9)$$

where I_1 , I_2 , and I_3 are defined as

$$I_1 = \int_0^\infty \ln(1 + c_j \gamma_B) f_{\gamma_B}(\gamma_B) F_{\gamma_E}(\gamma_B) d\gamma_B, \quad (10)$$

$$I_2 = \int_0^\infty \ln(1 + c_j \gamma_E) f_{\gamma_E}(\gamma_E) F_{\gamma_B}(\gamma_E) d\gamma_E, \quad (11)$$

$$I_3 = \int_0^\infty \ln(1 + c_j \gamma_E) f_{\gamma_E}(\gamma_E) d\gamma_E. \quad (12)$$

Substituting (6) and (7) into (10) and utilising [24, Equation (8.4.6.5)], I_1 is solved as

$$I_1 = D_B D_E \sum_{k=1}^{\beta_B} \sum_{m=1}^{\beta_E} b_{kB} b_{mE} \int_0^\infty G_{2,2}^{1,2} \left(\begin{matrix} 1, 1 \\ 1, 0 \end{matrix} \middle| c_j \gamma_B \right) \times G_{j,3j}^{3j,0} \left(\begin{matrix} l_{1B} - 1 \\ l_{2B} - 1 \end{matrix} \middle| \frac{E_B \gamma_B}{\mu_{jB}} \right) G_{j+1,3j+1}^{3j,1} \left(\begin{matrix} 1, l_{1E} \\ l_{1E}, 0 \end{matrix} \middle| \frac{E_E \gamma_B}{\mu_{jE}} \right) d\gamma_B. \quad (13)$$

With the aid of [25, Equation (21.02.04.0001)], (13) is evaluated in terms of the extended generalised bivariate Meijer-G function [7] as follows:

$$I_1 = D_B D_E \sum_{k=1}^{\beta_B} \sum_{m=1}^{\beta_E} b_{kB} b_{mE} \times G_{3j,j:j+1,3j+1;2,2}^{3j,0:3j,1;1,2} \left(\begin{matrix} l_{2B} \\ l_{1B} \end{matrix} \middle| \begin{matrix} 1, l_{1E} \\ l_{2E}, 0 \end{matrix} \middle| \begin{matrix} 1, 1 \\ 1, 0 \end{matrix} \middle| \frac{E_E \mu_{jB}}{E_B \mu_{jE}}, \frac{c_j \mu_{jB}}{E_B} \right). \quad (14)$$

Following a similar approach that we have used to compute I_1 , I_2 is obtained as

$$I_2 = D_B D_E \sum_{k=1}^{\beta_B} \sum_{m=1}^{\beta_E} b_{kB} b_{mE} \times G_{3j,j:j+1,3j+1;2,2}^{3j,0:3j,1;1,2} \left(\begin{matrix} l_{2E} \\ l_{1E} \end{matrix} \middle| \begin{matrix} 1, l_{1B} \\ l_{2B}, 0 \end{matrix} \middle| \begin{matrix} 1, 1 \\ 1, 0 \end{matrix} \middle| \frac{E_B \mu_{jE}}{E_E \mu_{jB}}, \frac{c_j \mu_{jE}}{E_E} \right). \quad (15)$$

Remark 1. The extended generalised bivariate Meijer-G function, which appears in (14) and (15), can be implemented in Mathematica using the code given in [26].

4 | SOP PERFORMANCE ANALYSIS

In the presence of passive eavesdropper, SOP is an important secrecy performance metric. SOP is defined as the probability that the instantaneous secrecy capacity is less than a given threshold rate, and is expressed as [12]

$$\begin{aligned} \text{SOP} &= P_r \{ C_s(\gamma_B, \gamma_E) < C_{th} \}, \\ &= \int_0^\infty f_{\gamma_E}(\gamma_E) F_{\gamma_B} \left(\gamma_E \Theta + \frac{\Theta - 1}{c_j} \right) d\gamma_E, \quad (16) \end{aligned}$$

where C_{th} is threshold secrecy capacity and $\Theta = \exp(C_{th}) \geq 1$. On substituting (6) and (7) into (16), the SOP is evaluated as

$$\begin{aligned} \text{SOP} &= \frac{D_B D_E E_E}{\mu_{jE}} \sum_{k=1}^{\beta_B} \sum_{m=1}^{\beta_E} b_{kB} b_{mE} \int_0^\infty G_{j,3j}^{3j,0} \left(\begin{matrix} l_{1E} - 1 \\ l_{2E}, -1 \end{matrix} \middle| \frac{E_E}{\mu_{jE}} \gamma_E \right) \\ &\times G_{j+1,3j+1}^{3j,1} \left(\begin{matrix} 1, l_{1B} \\ l_{2B}, 0 \end{matrix} \middle| \frac{E_B}{\mu_{jB}} \left(\gamma_E \Theta + \frac{\Theta - 1}{c_j} \right) \right) d\gamma_E. \quad (17) \end{aligned}$$

Now, using [24, Eq. (2.24.1.3)], (17) can be written as

$$\begin{aligned} \text{SOP} &= \frac{D_B D_E E_E \mu_{jB}}{E_B \mu_{jE} \Theta} \sum_{k=1}^{\beta_B} \sum_{m=1}^{\beta_E} \sum_{n=0}^{\infty} b_{kB} b_{mE} \frac{\left(\frac{-E_B(\Theta - 1)}{\mu_{jB} c_j} \right)^n}{n!} \\ &\times G_{4j+2,4j+2}^{3j+1,3j+1} \left(\begin{matrix} 0, n - l_{2B}, n, l_{1E} - 1 \\ l_{2E} - 1, n - 1, n - l_{1B}, n \end{matrix} \middle| \frac{\mu_{jB} E_E}{\mu_{jE} E_B \Theta} \right). \quad (18) \end{aligned}$$

Remark 2. Although the expression for SOP given by (18) is expressed in terms of an infinite series, it converges quickly for finitely small values of n , that is, $n = 8$ is sufficient for the convergence of this series. The proof of convergence of this infinite series is shown in Appendix.

5 | ASYMPTOTIC SOP ANALYSIS

To obtain useful insights into the system, we perform asymptotic SOP analysis in this section. Let us carefully observe (18) for high SNR on the main channel, μ_{jB} , and a fixed eavesdropper channel SNR, μ_{jE} .

5.1 | Heterodyne detection, $j = 1$

On substituting $j = 1$ in (18), the SOP is written as

$$\begin{aligned} \text{SOP} &= \frac{D_B D_E E_E \mu_{1B}}{E_B \mu_{1E} \Theta} \sum_{k=1}^{\beta_B} \sum_{m=1}^{\beta_E} \sum_{n=0}^{\infty} b_{kB} b_{mE} \frac{\left(\frac{E_B(1-\Theta)}{\mu_{1B} c_j} \right)^n}{n!} \times \\ &G_{6,6}^{4,4} \left(\begin{matrix} 0, n - \psi_{\text{mod}_B}^2, n - \alpha_B, n - k, n, \psi_{\text{mod}_E}^2 \\ \psi_{\text{mod}_E}^2 - 1, \alpha_E - 1, m - 1, n - 1, n - \psi_{\text{mod}_B}^2, n \end{matrix} \middle| \frac{\mu_{1B} E_E}{\mu_{1E} E_B \Theta} \right). \quad (19) \end{aligned}$$

Using Slater's theorem [27], the Meijer-G function in (19) can be represented in terms of the generalised hypergeometric function as follows:

$$\begin{aligned} G_{6,6}^{4,4} \left(\begin{matrix} \mathbf{a} \\ \mathbf{b} \end{matrix} \middle| \frac{\mu_{1B} E_E}{\mu_{1E} E_B \Theta} \right) &= \\ &\sum_{b=1}^4 \frac{\prod_{i=1}^4 \Gamma(a_b - a_i) \prod_{i=1}^4 \Gamma(1 - a_b + b_i)}{\prod_{i=5}^6 \Gamma(1 - a_b + a_i) \prod_{i=5}^6 \Gamma(a_b - b_i)} \\ &\times \left(\frac{\mu_{1B} E_E}{\mu_{1E} E_B \Theta} \right)^{a_b - 1} {}_6F_5 \left(1 - a_b + \mathbf{b}, (1 - a_b + \mathbf{a})^*, \frac{\mu_{1E} E_B \Theta}{\mu_{1B} E_E} \right), \quad (20) \end{aligned}$$

where $\mathbf{a} = [a_1, a_2, \dots, a_6] = [0, n - \psi_{\text{mod}_B}^2, n - \alpha_B, n - k, n, \psi_{\text{mod}_E}^2]$, $\mathbf{b} = [b_1, b_2, \dots, b_6] = [\psi_{\text{mod}_E}^2 - 1, \alpha_E - 1, m - 1, n - 1, n - \psi_{\text{mod}_B}^2, n]$, and $(\cdot)^*$ denotes that the terms $a_b = a_i$ are to be

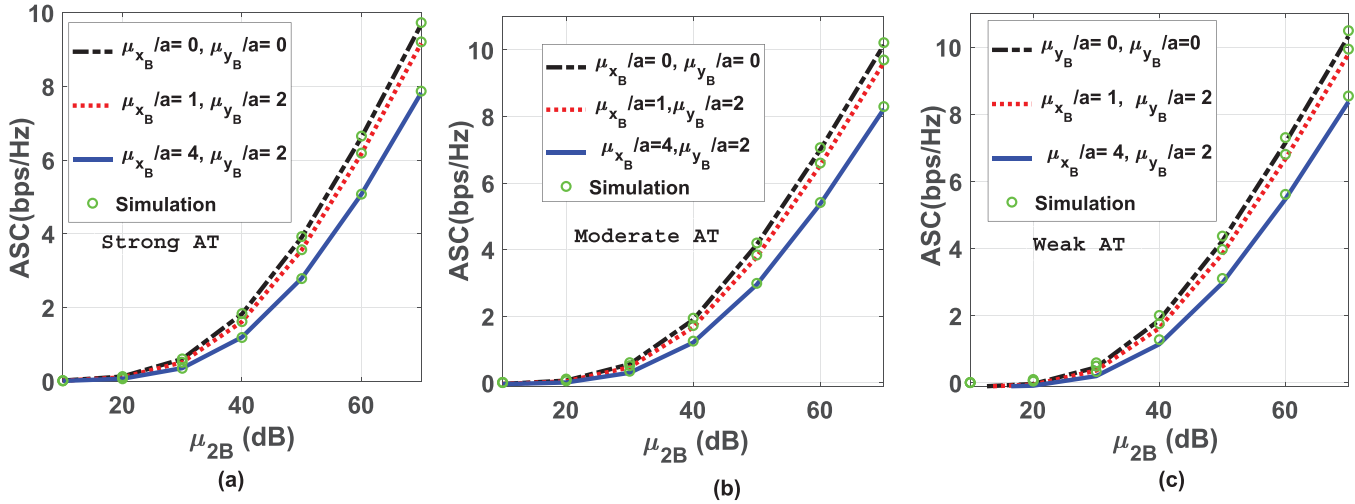


FIGURE 1 ASC as a function of electrical SNR on A-B link under strong to weak AT (Figure 1a–c) with IM/DD technique different values of $(\mu_{x_B}/a$ and $\mu_{y_B}/a)$ and with fixed $(\mu_{x_E}/a = 4$ and $\mu_{y_E}/a = 3)$ and equal jitter ($\sigma_x/a = 4$, $\sigma_y/a = 3$) on both links.

ignored. For high SNR (μ_{1B}), $\frac{\mu_{1E}E_B\Theta}{\mu_{1B}E_E} \rightarrow 0$ and consequently, ${}_6F_5(\cdot, \cdot, x) \rightarrow 1$. Therefore, the asymptotic SOP for HD, after some simplification, can be approximated as

$$\text{SOP} \approx D_B D_E \sum_{k=1}^{\beta_B} \sum_{m=1}^{\beta_E} \sum_{n=0}^{\infty} \frac{b_{kB} b_{mE} \left(\frac{E_B(1-\Theta)}{c_j} \right)^n}{n!} \times \left(\frac{\kappa_1}{\mu_{1B}^{n-a_1}} + \frac{\kappa_2}{\mu_{1B}^{n-a_2}} + \frac{\kappa_3}{\mu_{1B}^{n-a_3}} + \frac{\kappa_4}{\mu_{1B}^{n-a_4}} \right), \quad (21)$$

where $\kappa_b = \frac{\prod_{i=1}^4 \Gamma(a_b - a_i) \prod_{i=1}^4 \Gamma(1 - a_b + b_i)}{\prod_{i=5}^6 \Gamma(1 - a_b + a_i) \prod_{i=5}^6 \Gamma(a_b - b_i)} \left(\frac{E_E}{\mu_{1E} E_B \Theta} \right)^{a_b}$, $b = 1, 2, 3, 4$.

Now, putting the values of $[a_1, a_2, a_3, a_4] = [0, n - \psi_{\text{mod}_B}^2, n - \alpha_B, n - k]$ into (21) and observing that the dominant term in the asymptotic SOP expression given by (21) will correspond to the smallest power of μ_{1B} , the asymptotic slope of the SOP is given by $\delta = \min\{\psi_{\text{mod}_B}^2, \alpha_B, k\}$.

5.2 | IM/DD detection, $j = 2$

On substituting $j = 2$ in (18) and performing a similar asymptotic analysis as mentioned in the previous subsection, the asymptotic slope of the SOP for this case can be derived as $\delta = \min\{\psi_{\text{mod}_B}^2/2, k/2, \alpha_B/2\}$.

Remark 3. The asymptotic slope of the SOP for HD ($j = 1$) or IM/DD ($j = 2$) depends only on the AT and PE parameters of the main channel and is independent of the corresponding parameters on the eavesdropper channel for a given μ_{1E} and can be expressed as $\delta = \min\{\psi_{\text{mod}_B}^2/j, \alpha_B/j, k/j\}$.

6 | NUMERICAL RESULTS AND DISCUSSION

In this section, we present the analytical results and their validation using Monte Carlo simulation with the aid of Mathematica and MATLAB platform for the considered FSO system. The link parameter values are chosen from references [7, 16, 28]. The link parameters used are: link length $L = 1$ km, operational wavelength $\lambda = 785$ nm, and refraction structure parameter, $C_n^2 = (1.2 \times 10^{-13} m^{-2/3}, 10^{-11} m^{-2/3}, \text{ and } C_n^2 = 2.8 \times 10^{-14} m^{-2/3})$. These are utilised to compute the Rytov variance using $\sigma_R^2 = 1.23 C_n^2 (2\pi/\lambda)^{7/6} L^{11/6}$ that subsequently helps to obtain the effects of AT for both links as $(\alpha = 2.296; \beta = 2)$, $(\alpha = 4.2; \beta = 3)$, and $(\alpha = 8; \beta = 4)$ representing strong, moderate, and weak AT, respectively. The values of other parameters are chosen as $b_0 = 0.1079$, $\Omega = 1.3265$, $\rho = 0.596$, and $\phi_a - \phi_b = \pi/2$ [7, 15–28].

Figures 1 and 2 show the comparison of ASC performance under the strong to weak AT for different combination of boresight with jitter at a fixed $\mu_{jE} = 7$ dB and $w_z/a = 7$. We observe from Figure 1–c that as the boresight increases from $\{\mu_{x_B}/a, \mu_{y_B}/a\} = \{(0, 0)\}$ to $\{(1, 2)\}$ to $\{(4, 2)\}$, ASC performance deteriorates. This is because laser beam center is misaligned with respect to B's detector plane which consequently increases the fluctuation in instantaneous SNR on A-B link. Similar trends are reported for the HD case in Figure 2. Moreover, it can be seen from Figures 1 and 2 that HD ($j = 1$) technique provides superior ASC performance than IM/DD ($j = 2$) technique at the expense of increased cost and complexity. Figure 3a,b displays the SOP performance under the combined effect of strong to weak AT with boresight and jitter. SOP is plotted as a function of μ_{jB} with $\mu_{jE} = 10$ dB and 12 dB for $C_{tb} = 1$ and $w_z/a = 10$. The SOP performance is better at high μ_{jB} , whereas it degrades while moving from weak to strong AT. Further for SOP = 0.02 at $\mu_{jE} = 10$ dB, the required

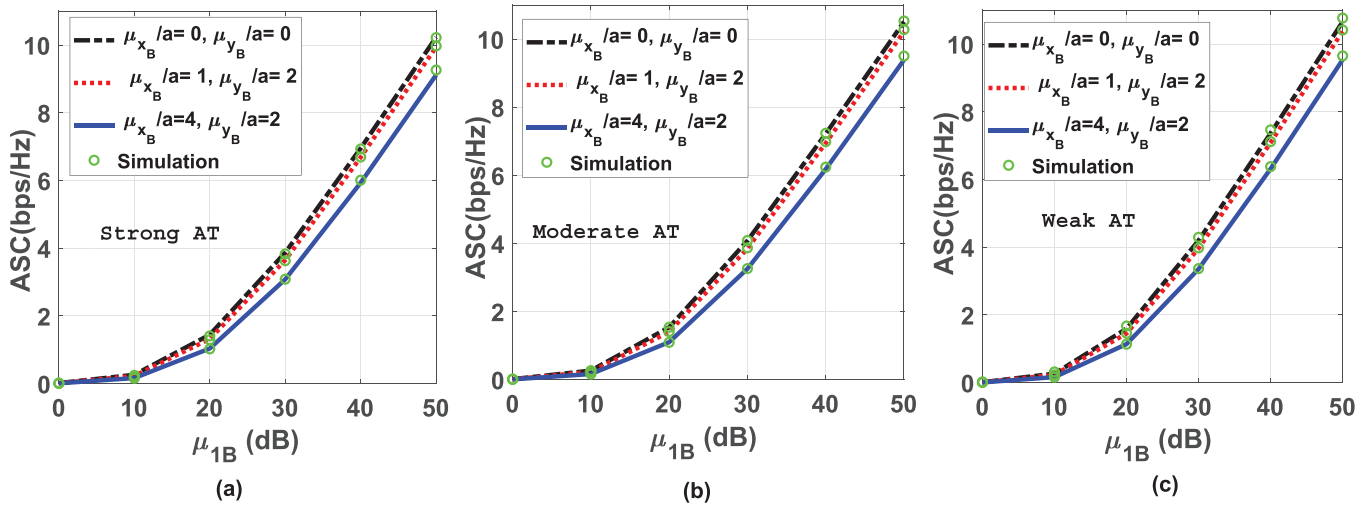


FIGURE 2 ASC as a function of electrical SNR on A-B link under strong to weak AT (Figure 2a-c) with HD technique different values of $(\mu_{x_B}/a$ and $\mu_{y_B}/a)$ and with fixed $(\mu_{x_E}/a = 4$ and $\mu_{y_E}/a = 3)$ and equal jitter ($\sigma_x/a = 4, \sigma_y/a = 3$) on both links.

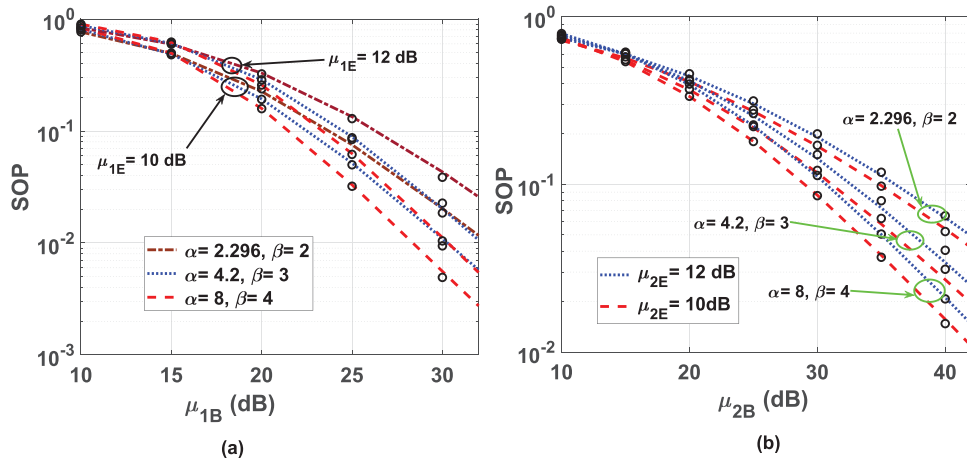


FIGURE 3 SOP versus electrical SNR on A-B link with equal value boresight ($\mu_{x_B}/a = \mu_{x_E}/a = 4$ and $\mu_{y_B}/a = \mu_{y_E}/a = 3$) and equal jitter ($\sigma_x/a = 1, \sigma_y/a = 2$) on both the links, (a) and (b) represent HD and IM/DD techniques, respectively.

$\mu_{2B} \approx 46$ dB for IM/DD and $\mu_{1B} \approx 30$ dB for HD. This points to an SNR penalty of around 16 dB for IM/DD.

In Figure 4, we compare the effect of change in boresight on the A-B link (for a fixed boresight on the A-E link $\mu_{x_E}/a = 4$ $\mu_{y_E}/a = 3$) on the ASC performance of HD and IM/DD techniques. The red curve indicates the ASC difference as the boresight on the A-B link is increased from $\{\mu_{x_B}/a, \mu_{y_B}/a\} = \{0, 0\}$ to $\{1, 2\}$ while the black curve indicates the ASC difference as the boresight on the A-B link is increased from $\{\mu_{x_B}/a, \mu_{y_B}/a\} = \{1, 2\}$ to $\{4, 2\}$. We observed that the ASC difference is higher for HD compared to IM/DD upto an SNR of $\mu_{1B} = \mu_{2B} = 46$ dB while moving from $\{\mu_{x_B}/a, \mu_{y_B}/a\} = \{0, 0\}$ to $\{1, 2\}$ and the converse is true above SNR. Similar trends are noticed while the A-B link boresight moving from $\{\mu_{x_B}/a, \mu_{y_B}/a\} = \{1, 2\}$ to $\{4, 2\}$. This indicates that IM/DD is more resistant to change in boresight compared to HD tech-

nique upto a certain SNR while the converse is true for higher SNR. Figure 5 illustrates that when A-E link SNR changes from 12 to 10 dB, SOP performance improves for both detection techniques but HD shows better SOP improvement than IM/DD for $\mu_{1B} = \mu_{2B} \approx 4$ dB to ≈ 23 dB under strong AT; the converse is true for the remaining SNR range.

Figures 6 and 7 present the SOP and ASC performance, respectively, under the combined effects of AT and PEs (jitter and boresight), for different values of ρ . It is seen from the figures that the ASC and SOP performance improves with the increase in the ρ values. This is because for higher values of ρ , more amount of scattering power will be coupled to the LOS component, consequently decreasing the turbulence intensity. This observation of improved secrecy performance with increasing ρ is also in line with the results reported in [15].

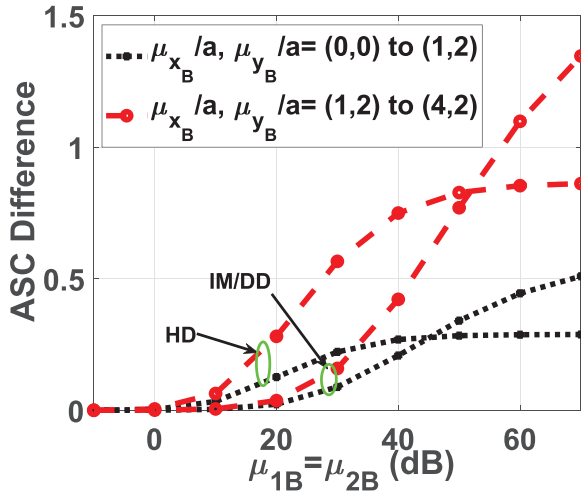


FIGURE 4 Comparison of the effect of change in boresight on the A-B links (for fixed boresight on the A-E link and equal jitter $\sigma_x/a = 1, \sigma_y/a = 2$) on the ASC performance of HD and IM/DD.

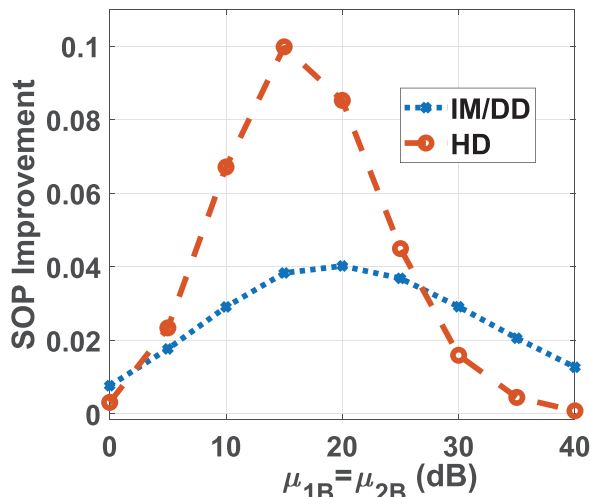


FIGURE 5 Comparison of the effect of change in electrical SNR on the A-E link (12–10 dB) on SOP performances of HD and IM/DD for equal boresight ($\mu_{xB}/a = \mu_{xE}/a = 4$ and $\mu_{yB}/a = \mu_{yE}/a = 3$) and equal jitter ($\sigma_x/a = 1$ and $\sigma_y/a = 2$) on both the links.

7 | CONCLUSIONS

In this work, we developed generalised expressions for the ASC and SOP which are important and useful for system designers for conducting security analyses of FSO communication systems under AT and non-zero boresight PEs. Useful insights about the secrecy performance are obtained through the asymptotic SOP analysis and simulation results under different detection techniques.

ACKNOWLEDGEMENTS

Science and Education Research Board (SERB), Project File No. ECR/2018/000797; Department of Science and Technology (DST), Government of India.

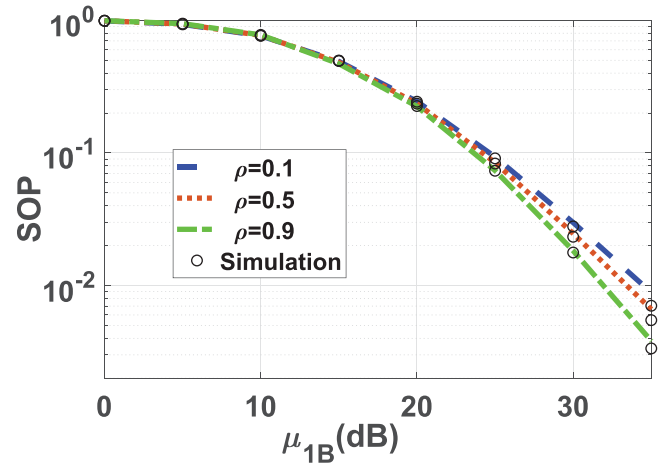


FIGURE 6 SOP versus electrical SNR on A-B link with equal value boresight ($\mu_x/a = 1$ and $\mu_y/a = 2$) and jitter ($\sigma_x/a = 1, \sigma_y/a = 2$) on both the links for HD technique.

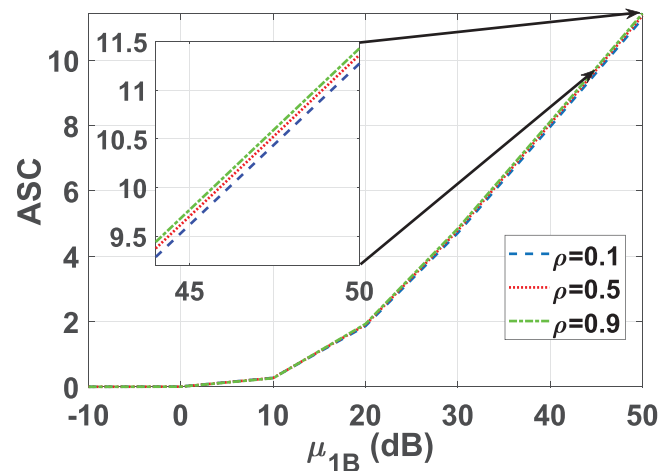


FIGURE 7 ASC versus electrical SNR on A-B link with equal value boresight ($\mu_x/a = 1$ and $\mu_y/a = 2$) and jitter ($\sigma_x/a = 1, \sigma_y/a = 2$) on both the links for HD technique.

ORCID

Yun Ai <https://orcid.org/0000-0002-3409-8152>

REFERENCES

1. Khalighi, M., Uysal, M.: Survey on free space optical communication: A communication theory perspective. *IEEE Commun. Surveys Tuts.* 16(4), 2231–2258 (2014)
2. Varotsos, G., et al.: SIMO optical wireless links with nonzero boresight pointing errors over M. modeled turbulence channels. *Elsevier Opt. Commun.* 403, 391–400 (2017)
3. Ghassemlooy, Z., et al.: *Optical Wireless Communications: System and Channel Modelling with MATLAB*. CRC Press, New York (2012)
4. Boluda-Ruiz, R., et al.: Novel approximation of misalignment fading modeled by Beckmann distribution on free-space optical links. *Opt. Exp.* 24(20), 22635–22649 (2016)
5. Yang, F., et al.: Free-space optical communication with nonzero boresight pointing errors. *IEEE Trans. Commun.* 62(2), 713–725 (2014)
6. Kim, I., et al.: Wireless optical transmission of fast ethernet, FDDI, ATM, and ESCON protocol data using the terralink laser communication system. *Opt. Eng.* 37(12), 3143–3155 (1998)

7. Ansari, I., et al.: Performance analysis of free-space optical links over mllaga (M) turbulence channels with pointing errors. *IEEE Trans. Wireless Commun.* 15(1), 91–102 (2016)
8. Aghajanzadeh, S., Uysal, M.: Outage analysis of hybrid-ARQ protocols in coherent free-space optical communications. In: 2011 IEEE 22nd International Symposium on Personal, Indoor and Mobile Radio Communication, Toronto, ON, 2011, pp. 1773–1777
9. Lopez-Martinez, F., et al.: Physical-layer security in free-space optical communications. *IEEE Photon J.* 7(2), 1–14 (2015)
10. Bloch, M., et al.: Wireless information-theoretic security. *IEEE Trans. Inf. Theory* 54(6), 2515–2534 (2008)
11. Lei, H., et al.: On physical-layer security over SIMO generalized-K fading channels. *IEEE Trans. Veh. Technol.* 65(9), 7780–7785 (2016)
12. Mathur, A., et al.: On physical layer security of α - η - κ - μ fading channels. *IEEE Commun. Lett.* 22(10), 2168–2171 (2018)
13. Ai, Y., et al.: On physical layer security of double Rayleigh fading channels for vehicular communications. *IEEE Wireless Commun. Lett.* 7(6), 1038–1041 (2018)
14. Ai, Y., et al.: Physical layer security of hybrid satellite-FSO cooperative systems. *IEEE Photon J.* 11(1), 1–14 (2019)
15. Saber, M., Sadough, S. M. S.: On secure free-space optical communications over Mallaga turbulence channels. *IEEE Wireless Commun. Lett.* 6(2), 274–277 (2017)
16. Saber, M., et al.: Physical-layer security analysis of mixed SIMO SWIPT RF and FSO fixed-gain relaying systems. *IEEE Sys. J.* 13(3), 2851–2858 (2019)
17. Pattanayak, D., et al.: Physical layer security of a two way relay based mixed FSO/RF network in the presence of multiple eavesdroppers. *Opt. Commun.* 463, 125429 (2020)
18. Ai, Y., et al.: Secrecy enhancement of RF backhaul system with parallel FSO communication link. *Opt. Commun.* 475, 126193 (2020)
19. Wyner, A.: The wire-tap channel. *Bell Syst. Tech. J.* 54(8), 1355–1387 (1975)
20. Gappmair, W.: Novel results on pulse-position modulation performance for terrestrial free-space optical links impaired by turbulent atmosphere and pointing errors. *IET Commun.* 6(10), 1300–1305 (2012)
21. Jurado-Navas, A., et al.: A unifying statistical model for atmospheric optical scintillation. Numerical simulations of physical and engineering processes 181 (2011)
22. Saxena, P., et al.: BER of an optically pre-amplified FSO system under Mllaga turbulence, pointing errors, and ASE noise. In: 2017 IEEE 28th Annual International Symposium on Personal, Indoor, and Mobile Radio Communication (PIMRC), Montreal, QC, 1–6 (2017)
23. Mathur, A., et al.: Secrecy performance of correlated α - μ fading channels. *IEEE Commun. Lett.* 23(8), 1323–1327 (2019)
24. Prudnikov, A., et al.: Integrals and Series. Volume 3: More Special Functions. Gordon and Breach Science Publisher, Amsterdam, Paris, New York (1989)
25. Wolfram, S.: A wolfram web resource. <http://functions.wolfram.com/HypergeometricFunctions/MeijerG/>. Accessed 3 Jan 2020
26. Ansari, I., et al.: A. new formula for the BER of binary modulations with dual-branch selection over generalized-K composite fading channels. *IEEE Trans. Commun.* 59(10), 2654–2658 (2011)
27. Roach, K.: Meijer g function representations. *Int. Conf. Symbolic Algebraic Computation. ISSAC 97. Association for Computing Machinery, New York* 205–211 (1997).
28. Jurado-Navas, A., et al.: Impact of pointing errors on the performance of generalized atmospheric optical channels. *Opt. Exp.* 20(11), 12550–12562 (2012)
29. Arfken, G., Weber, H.: Integral Transforms Mathematical Methods for Physicists. 4th edn., pp. 846–919. Academic Press, Boston (1995)

How to cite this article: Verma GD, Mathur A, A Yun, M Cheffena. Secrecy performance of FSO communication systems with non-zero boresight pointing errors. *IET Commun.* 2021;15:155–162. <https://doi.org/10.1049/cmu2.12068>

APPENDIX A: PROOF OF SERIES CONVERGENCE OF EQUATION (18)

In order to show the convergence of the infinite series in (18), we utilise the Cauchy Ratio Test proposed in [29]. On taking the ratio of the $(n + 1)$ th and n th terms given by (A.1) and (A.2), respectively, shown at the top of the page, and further applying the Cauchy Ratio Test [29] to (A.3) shown at the top of the page, we observe that

$$a_n = \frac{D_B D_E E_E \mu_{jB}}{E_B \mu_{jE} \Theta} \frac{\left(\frac{-E_B(\Theta-1)}{\mu_{jB} c_j}\right)^n}{n!} \sum_{k=1}^{\beta_B} \sum_{m=1}^{\beta_E} b_{kB} b_{mE} G_{4j+2, 4j+2}^{3j+1, 3j+1} \left(\begin{matrix} 0, n - l_{2B}, n, l_{1E} - 1 \\ l_{2E} - 1, n - 1, n - l_{1B}, n \end{matrix} \middle| \frac{\mu_{jB} E_E}{\mu_{jE} E_B \Theta} \right), \quad (\text{A.1})$$

$$a_{n+1} = \frac{D_B D_E E_E \mu_{jB}}{E_B \mu_{jE} \Theta} \frac{\left(\frac{-E_B(\Theta-1)}{\mu_{jB} c_j}\right)^{n+1}}{(n+1)!} \sum_{k=1}^{\beta_B} \sum_{m=1}^{\beta_E} b_{kB} b_{mE} G_{4j+2, 4j+2}^{3j+1, 3j+1} \left(\begin{matrix} 0, n+1 - l_{2B}, n+1, l_{1E} - 1 \\ l_{2E} - 1, n, n+1 - l_{1B}, n+1 \end{matrix} \middle| \frac{\mu_{jB} E_E}{\mu_{jE} E_B \Theta} \right), \quad (\text{A.2})$$

$$\frac{a_{n+1}}{a_n} = \frac{E_B(1-\Theta)}{\mu_{jB} c_j (n+1)} \frac{\sum_{k=1}^{\beta_B} \sum_{m=1}^{\beta_E} b_{kB} b_{mE} G_{4j+2, 4j+2}^{3j+1, 3j+1} \left(\begin{matrix} 0, n+1 - l_{2B}, n+1, l_{1E} - 1 \\ l_{2E} - 1, n, n+1 - l_{1B}, n+1 \end{matrix} \middle| \frac{\mu_{jB} E_E}{\mu_{jE} E_B \Theta} \right)}{\sum_{k=1}^{\beta_B} \sum_{m=1}^{\beta_E} b_{kB} b_{mE} G_{4j+2, 4j+2}^{3j+1, 3j+1} \left(\begin{matrix} 0, n - l_{2B}, n, l_{1E} - 1 \\ l_{2E} - 1, n - 1, n - l_{1B}, n \end{matrix} \middle| \frac{\mu_{jB} E_E}{\mu_{jE} E_B \Theta} \right)}. \quad (\text{A.3})$$

$$L = \lim_{n \rightarrow \infty} \left| \frac{a_{n+1}}{a_n} \right| \rightarrow 0. \quad (\text{A.4})$$

Therefore, the infinite series in (18) converges because $L < 1$ by the application of the Cauchy Ratio Test.